2025 IEEE/SICE International Symposium on System Integration (SII)
January 21-24, 2025, Munich, Germany

Real-Time Estimation of Shoulder Motion Intention with a Neuromusculoskeletal Model and a Neural Network*

Jorge Andreé Orellana Wong, Satoshi Nishikawa, *Member, IEEE*, Kazuo Kiguchi, *Senior Member, IEEE*

***Abstract*—The development of robotic exoskeletons for human motion assistance and rehabilitation has intensified the need for efficient methods to discern users' motion intentions, particularly for complex upper limb movements. The shoulder joint poses the most significant challenge due to its anatomical complexity, multi-degree-of-freedom (DoF) movements, and variable muscle function. Consequently, real-time estimation of shoulder joint motion intentions remains the least explored. Existing prediction methods often fail to address the shoulder's range of motion, as many models are restricted to below the shoulder level or rely on computationally intensive physiological parameters unsuitable for real-time applications. The shoulder's varying moment arm further complicates signal normalization and accuracy. To overcome these challenges, we propose a novel approach combining a Neuromusculoskeletal Model with a Multilayer Perceptron (MLP). This method leverages biological insights from the model to improve neural network performance, focusing exclusively on regression for real-time predictions. The method inputs include sEMG signals from shoulder muscles and shoulder angle data. These sEMG signals are preprocessed and integrated into the Neuromusculoskeletal Model, which incorporates activation dynamics, contraction dynamics, and musculoskeletal measurements. By correlating skeletal measurements with humeral elevation, the method reduces computational complexity and calculates muscle torques, which are then used by the MLP to estimate humeral acceleration. This approach effectively addresses normalization issues by correlating shoulder angle, sEMG data, and estimated torques with humeral acceleration.**

I. Introduction

Recent advancements in robotics technology have significantly impacted the fields of medicine and welfare, particularly in response to the growing elderly population and the increasing prevalence of upper-limb impairments due to strokes [1][2], sports injuries, traumas, and occupational injuries [3]. Consequently, there is a critical demand for upper-limb assistive devices that facilitate basic daily activities and support rehabilitation. A crucial requirement for these assistive devices is their ability to adapt to the patient's motion intentions to provide effective rehabilitation and assistance.

Surface electromyography (sEMG) is the predominant biological signal for interpreting a user's motion intentions. Research on motion intention prediction from sEMG signals can be classified into two primary approaches: classification and regression. Among these, regression, particularly continuous regression, has received less attention [4][5]. Continuous regression methods are further divided into Model-Based (MB) and Model-Free (MF) approaches.

Model-Free (MF) approaches leverage machine learning or deep learning techniques to extract advanced features from sEMG signals, establishing complex, nonlinear relationships between these features and the motion intention. The primary advantage of MF approaches lies in their capacity to handle intricate signal features and adapt to various motion patterns. However, they often overlook the physiological effects of the sEMG signal, which complicates generalization across different individuals, as they heavily rely on the training data [4][6].

In contrast, Model-Based (MB) approaches utilize physiological principles to translate sEMG signals into muscle-tendon forces by incorporating activation dynamics and contraction dynamics. These forces are then applied to musculoskeletal models and equations of motion to predict joint kinematics and dynamics [7][8]. The strength of MB approaches lies in their ability to elucidate the relationship between sEMG signals and motion intention through a physiological framework. Nevertheless, these models face challenges due to individual physiological variations, and much of the existing research is based on Hill-type muscle models and cadaver studies, which may not accurately represent patient conditions [4][9]. To address these challenges MB methods often require extensive parameter

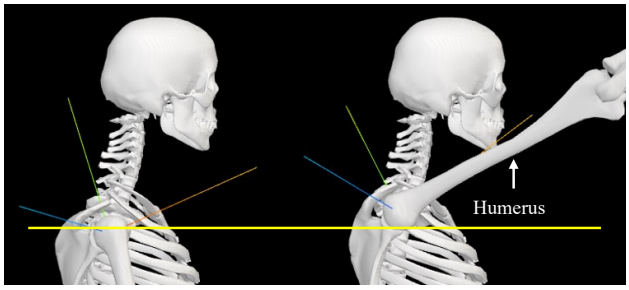

Fig. 1. Shoulder Axis Rotation Displacement using OpenSim 4.4 [17][18]

* This work was supported by JST [Moonshot R&D] [Grant Number JPMJMS2034].

Jorge A. Orellana Wong is with Department of Mechanical Engineering, Kyushu University, Fukuoka, 744 Motooka Nishi-ku, Japan (e-mail: orellana.wong.jorge.188@s.kyushu-u-ac.jp).

Satoshi Nishikawa is with Department of Mechanical Engineering, Kyushu University, Fukuoka, 744 Motooka Nishi-ku, Japan (e-mail: nishikawa@mech.kyushu-u.ac.jp).

Kazuo Kiguchi is with Department of Mechanical Engineering, Kyushu University, Fukuoka, 744 Motooka Nishi-ku, Japan (phone: +81-92-802-3236; email: kiguchi@mech.kyushu-u.ac.jp).

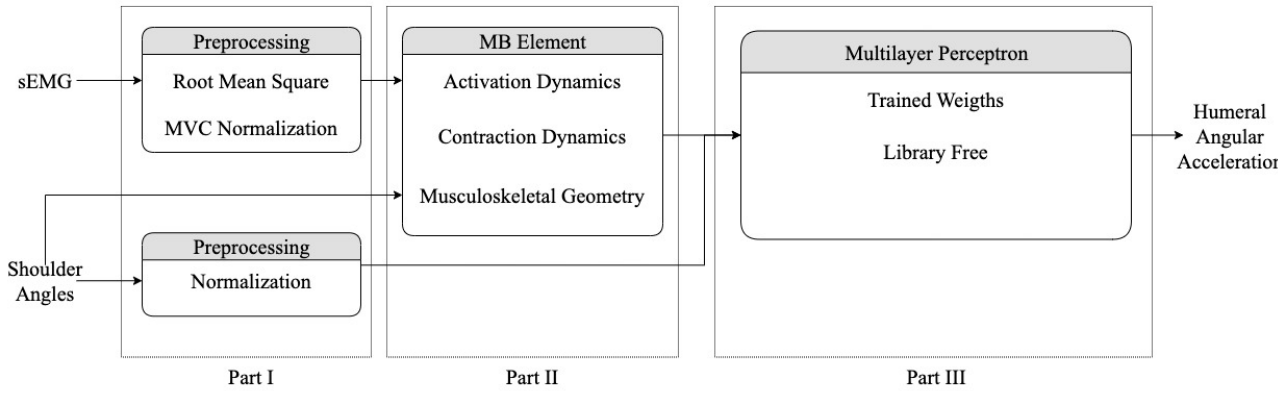

Fig.2. Method Architecture

optimization to ensure accurate real-time kinematic and dynamic intention predictions.

For sEMG-based motion intention prediction, the shoulder is the least studied among upper-limb joints. This limited research is due to the shoulder's high kinematic complexity, which affords it an extensive range of motion [10]. Specifically, the shoulder's movement is characterized by a three-axis rotational clavicle and scapula with five degrees of freedom, allowing it to displace the humeral head based on humeral position, as shown in Fig. 1 [11]. Research that endeavors to explore it stays below shoulder level [2] [12][13]. In contrast, research that attempted shoulder motion prediction that used similar kinematic, dynamic, and physiological models is predominantly limited to single plane movements below shoulder level [14] and is not real-time [15][16].

Furthermore, the shoulder range of motion introduces variability in muscle function. As the humerus moves from below to above the joint, shoulder muscles perform varying or simultaneous tasks depending on the humeral position. This variability complicates the correlation between sEMG amplitude and actual shoulder motion intention. Additionally, muscle length changes—where some muscles are stretching, others are shortening—can cause significant variation in the maximal voluntary contraction of shoulder muscles [19][20].

Research specifically targeting shoulder motion intention is sparse [4], and existing models tend to focus on predicting shoulder angle positions rather than the subject's motion intention [15][16]. Furthermore, most studies addressing shoulder motion intention are in an upper limb assist device environment that utilizes force sensors to determine the user's motion intention [21][22].

This study aims to develop a novel real-time method for estimating shoulder motion intention by combining a neuromusculoskeletal model with a MLP. This integration enhances the flexibility of the MLP by reducing its reliance on training data and tailoring the neuromusculoskeletal model to the specific physiology of the subject. Additionally, the musculoskeletal model proposed utilizes bone orientation correlation with humeral elevation to reduce computational complexity and optimize it for real-time application. Another function of the MLP is correlating the sEMG, shoulder angle position, calculated torques, and humeral acceleration, allowing the method to reach the full shoulder range of motion and avoid the sEMG normalization problem. The method is structured into three components: biological and non-biological signal preprocessing, a neuromusculoskeletal model, and a MLP, as shown in Fig. 2.

The organization of this paper is as follows: Section II presents the neuromusculoskeletal model, Section III discusses the MLP, Section IV details the experimental setup, Section V exhibits the results and discussion, and Section VI concludes the study.

II. Neuromusculoskeletal Model

A. Overview

The proposed method is divided into three parts, as shown in Fig. 2. Initially, the activation dynamics component will transform the sEMG feature extraction into muscle activation. Subsequently, the contraction dynamics model will take muscle activation with other muscle-related data and determine the muscle forces. Finally, all moment arms will be derived from the musculoskeletal model, and with muscle forces, it will compute the muscle torque in their origin and insertion.

B. Signal Preprocessing

The sEMG signal measures the integration of action potentials from multiple muscle fibers containing a wide range of frequencies. The relevant aspects needed from the sEMG signal are the timing, intensity, and activation shape. The two most used methods are rectification and low pass filtering or root mean square (RMS) [23][24]. After applying RMS, the best way to relate this feature to mechanical events is by normalizing over the maximal voluntary contraction (MVC). All sEMG signals are processed with RMS and then normalized based on MVC.

C. Activation Dynamics

Activation and deactivation dynamics are the processes that describe the delay between muscle force development and relaxation, which is a characteristic of the excitation-contraction coupling [25]. This delay occurs primarily because of calcium dynamics and cross-bridge attachment and detachment [26]. For activation dynamics, the Zajac model can be employed with the following differential equation

$$\frac{da(\tau)}{dt} + \left[\frac{1}{\bar{\tau}_{\text{act}}} \cdot \left(\beta + [1-\beta] \cdot e(\tau)\right)\right] \cdot a(\tau) = \left(\frac{1}{\bar{\tau}_{\text{act}}}\right) \cdot e(\tau) \quad (1)$$

where $e(\tau)$ represents the sEMG signa, $a(\tau)$ represents the activation dynamics, τ_{act} represents the time delay in muscle activation, and β represents the activation and deactivation time delay ratio. Additionally, time and delay parameters have been normalized with a time scale parameter of 0.1 described by Zajac. Equation (1) behaves like a low pass filter that introduces a delay between the neural excitation and muscle activation. One of the key aspects of this model is that activation rate is always bigger that the deactivation rate, also every muscle has its own unique activation and deactivation rates.

Equation (1) requires that the sEMG signal gets defined as an equation. The model uses three samples to generate a line fitting to determine *e(t)* and normalized the time variable to get *e(τ)*. Finally, the model can solve equation (1) by numerical integration with the Runge-Kutta algorithm. For activation, deactivation, muscle fiber length, optimal isometric force, and maximum optimal fiber velocity, the model can operate with the information from [14][17][18] on OpenSim 4.4.

D. Contraction Dynamics

Muscle contraction dynamics can be represented through two primary modeling approaches: physiological models and phenomenological models. Physiological models, while detailed, often entail substantial computational complexity, particularly when analyzing a large number of muscles. In contrast, phenomenological models, such as the Hill-type model, are preferred for their computational efficiency. The Hill-type model is widely used due to its ability to describe muscle dynamics with a single differential equation [8].

The force generated by the contractile element of the muscle fiber can be estimated with a Hill-type model. This model incorporates a length-dependent force component, a velocity-dependent force component, activation dynamics, and the maximum isometric muscle fiber force. Consequently, the muscle fiber force given by:

$$F_m(t) = f(l) f(v) a(t) F_{om} \quad (2)$$

where $f(l)$ represents the length-dependent force component, $f(v)$ represents velocity-dependent force component, $a(t)$ represents the activation dynamics component, and F_{om} represents the isometric muscle fiber force.

1) Muscle Force Change on Length

The length-dependent muscle fiber force is divided into active and passive components. The active component generates force when the muscle is activated, while the passive component resists stretching beyond the muscle's resting length. The active force behavior, as described by Gordon [27], is characterized by an initial absence of force at very short lengths, an increase in force with length until reaching a plateau, and a subsequent decrease in force to zero at longer lengths [28]. To estimate the active component the simplified model presented by Rockenfeller *et al*. [28] can be calculated. Conversely, the passive element exhibits minimal force at short lengths, increasing exponentially once the muscle fiber exceeds its optimal length. For this part, the estimation can be performed with Schutte's formulation [29]. The combination of these active and passive elements is represented by:

$$F_m(l) = \left(f_{\text{act}}(l) * a(t) + \frac{e^{10(l-1)}}{e^5}\right) F_{om} \quad (3)$$

where f_{act} represents the active component force, *a(t)* represents the activation dynamics, l represents the muscle fiber length, and F_{om} represents the isometric muscle fiber force.

2) Muscle Force Change on Velocity

The velocity-dependent component of muscle force follows Hill's formulation, which posits that the rate of energy liberation is proportional to the change in force [30]. The velocity-dependent component computation can be calculated with the modified version of Hill's equation, as presented by Buchanan *et al*. [8], which integrates both the force-length and force-velocity relationships to determine the force during concentric contractions based on fiber velocity. This is given by:

$$F_v = \frac{F_m(l) \cdot b - a \cdot v_m}{b + v_m} \quad (4)$$

where v_m represents muscle fiber velocity, and the constants a and b are specified by Hill as 399 and 0.331, respectively. Since muscles can contract concentrically and eccentrically, an additional equation was required. The description of force-velocity during an eccentric contraction can be performed with Aubert's model [32][33]. The equation is described as:

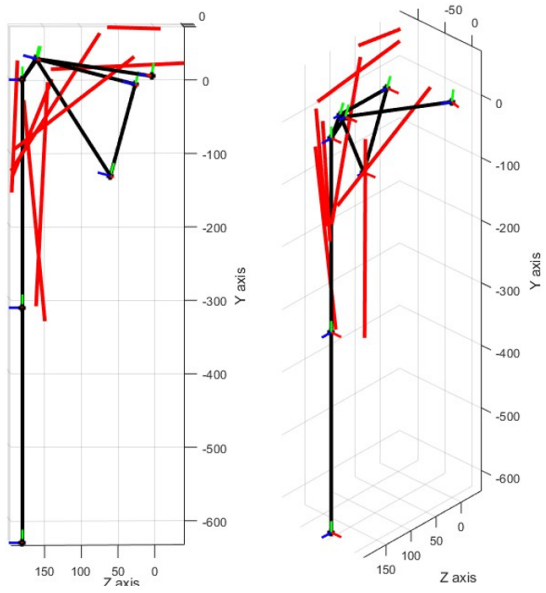

Fig.3. Musculoskeletal Model. Graph model using MATLAB [31]

NOTE: The redlines are the muscles picked, and the black lines represents the bones on the upper limb

$$F_v = 1.8 - 0.8 \cdot \frac{1 + \frac{v}{v_{\max}}}{1 - 7.56 \cdot \frac{0.25 \cdot v}{v_{\max}}} \quad (5)$$

where v_{max} denotes the maximum optimal fiber velocity at which force is zero, and v represents the fiber velocity.

E. Musculoskeletal Geometry

A detailed musculoskeletal geometry model is essential for computing the muscle torques on each joint. This geometrical model must fulfill several functions: it should define the rotational axes of all involved bones, specify bone dimensions, and provide the origin and insertion points of each muscle, along with their force trajectories. Additionally, the model is required to be in a standing position with the shoulder and elbow relaxed. The model can utilize the geometry developed by Wood *et al.* [34][35], the bone orientation in standing posture described by Matsumura *et al*. [36], and the kinematic information from Ludewig *et al.* [39].

The advantage of this geometry is that it accurately describes the rotational axes for the sternoclavicular, acromioclavicular, and glenohumeral joints and includes data on muscle origin and insertion locations, as well as linearized force trajectories. Moreover, the standing posture is an easy reference when testing the method. Furthermore, the bone size can be adjusted based on the subject height using data from [37][38]. Also, one of the primary difficulties is accurately modeling clavicle and scapula kinematics during humeral movements. The proposed geometry derives bone positions from non-biological signals by correlating bone orientations with humeral elevation and horizontal abduction. This approach is advantageous because it avoids the computationally intensive process of integrating sample-by-sample data to determine bone positions and orientations. The model can operate with the trajectory curves described by Ludewing *et al.* [39]

With the musculoskeletal model and shoulder angle measurements, it can determine the position of all bones, which allows us to calculate the differences in fiber length. From this, the model can derive fiber length and velocity. Concurrently, sEMG measurements of shoulder muscles provide data on muscle activation levels. Combining muscle activation with fiber length and velocity measurements enables the computation of muscle forces. By applying these muscle forces within the musculoskeletal model, the proposed method can ultimately derive the torques at the origin and insertion points of the muscles, thereby providing a comprehensive analysis of joint torques.

III. Neural Network

The neural network employed will customize the neuromusculoskeletal model to the specific physiology of the subject. To achieve accurate and rapid shoulder motion estimation, the proposed method can utilize a MLP architecture with hidden layers, utilizing the hyperbolic tangent (tanh) function as the activation function. The MLP receives as inputs the sEMG features from the shoulder muscles, normalized shoulder angles, and torques at the origins and insertions of each muscle. The MLP will predict the angular acceleration of the humerus along each axis.

The method preprocesses all non-biological data with a zero-delay fourth-order Butterworth filter. The filtering step was crucial to prevent the MLP from learning the noise present in the signal. The training of the MLP utilizes the supervised method and can use the Adam optimization algorithm with an exponential decay learning rate to accelerate the learning process. Moreover, the MLP can employ TensorFlow's Keras library in Python 3 with the default parameters for this optimization algorithm. One of the possible challenges of using a neural network library is the computational time required to use the library to make a single prediction; it can narrow the time to process the MB part. Therefore, the proposed method utilizes a second MLP. This second MLP's main characteristic is only for prediction. It does not use a neural network library. Instead, it used the learned weights and hyperparameters from the initial MLP to achieve quicker predictions.

IV. Experiment

An experiment was conducted to evaluate shoulder motion intention accuracy and the computing time of the proposed method. The experiment recruited three healthy male participants; the subjects' information is in Table 1. The experimental protocol involved recording sEMG signals from eight shoulder muscles, as listed in Table 2, while the subjects performed specified exercises. Total shoulder flexion, horizontal shoulder abduction, and external shoulder rotation angles were measured in degrees with MyoMotion sensors (Noraxon). The sEMG signals were measured using Ultium sensors (Noraxon) with a sampling frequency of 2000 Hz, while shoulder angles and accelerations were measured using MyoMotion sensors (Noraxon). Ultium sensors incorporate a high pass filter, and a low pass filter set at 10 Hz and 500 Hz. The sensor placement and axis reference are shown in Fig. 4.

Before the exercises, MVC was measured for each muscle by following the Kelly *et al*. protocol [20]. The experiment exercises selected were shoulder flexion, scaption, and shoulder abduction, as described by Ludewig *et al*. [39]. These exercises were performed twelve times each, with a duration of approximately two seconds per repetition and a two-minute rest period between exercises to mitigate fatigue.

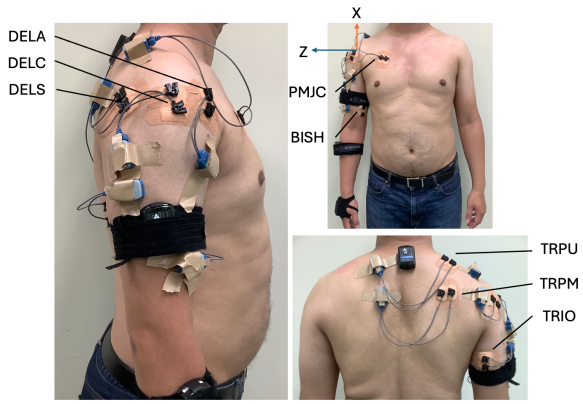

Fig.4. Sensor Placement

TABLE I. SUBJECTS RELEVANT INFORMATION

Subjects	*Sex*	*Age*	*Heigh (cm)*	*Weight (kg)*	*Hand Dominance*
S1	M	24	183	85	Right Hand
S2	M	28	183	95	Left Hand
S3	M	30	166	65	Right Hand

TABLE II. SENSORS PLACED

Sensor	*Type*	*Location*	*Measurement*
1	Ultium	Biceps Short Head (BISH)	sEMG
2	Ultium	Deltoid Acromial (DELA)	sEMG
3	Ultium	Deltoid Clavicular (DELC)	sEMG
4	Ultium	Deltoid Spinal (DELS)	sEMG
5	Ultium	Pectoral Clavicular Part (PMJC)	sEMG
6	Ultium	Triceps Long Head (TRIO)	sEMG
7	Ultium	Trapezius Medial (TRPM)	sEMG
8	Ultium	Trapezius Descend (TRPU)	sEMG
9	MyoMotion	Upper Thoracic Vertebra	SA, AA
10	MyoMotion	Right Upper Arm	SA, AA
11	MyoMotion	Right Forearm	EA, AA
12	MyoMotion	Right Hand	HA, AA

NOTE: The SA stand for shoulder angles, EA for elbow angles, HA for hand angle and AA for acceleration.

Subsequent data collection involved segmenting the data by exercise cycle, which got further divided into training and testing sets for the MLP, with a split of 80% for training and 20% for testing. The MLP's architecture was tested with three hidden layers: six times the number of inputs, three times the number of inputs, six times the number of inputs and a final layer of three neurons. The MLP input-out dimension is 66 inputs 3 outputs.

The training dataset was preprocessed as follows. The sEMG signals were root mean squared with a 200 ms window and normalized, while shoulder angles were filtered using a fourth-order Butterworth low pass filter with a 0.4 Hz cutoff frequency. The difference in performance with and without filter can be observed in Table 3. The processed signals, including sEMG features, normalized angles, and normalized torques, were input into an MLP for training. The target output was the angular acceleration derived from the accelerometer data. The testing set was input into the method one sample at a time. In order to evaluate the method's capacity for real-time, the method's processing time for each sample was recorded. Additionally, the predicted data was compared with the actual accelerometer data using the root mean square error metric.

V. RESULTS AND DISCUSSION

The comparison between the predicted humeral acceleration and the one measured is presented in Fig. 5. Additionally, a comparison is made with normalized total flexion and normalized deltoid acromial feature. As shown in Fig. 5, the predicted acceleration almost matches the behavior of the actual acceleration, deviating predominantly at peaks in the normalized deltoid acromial feature and extreme total flexion positions. The method's accuracy was assessed using the root mean square error (RMSE) across each shoulder axis.

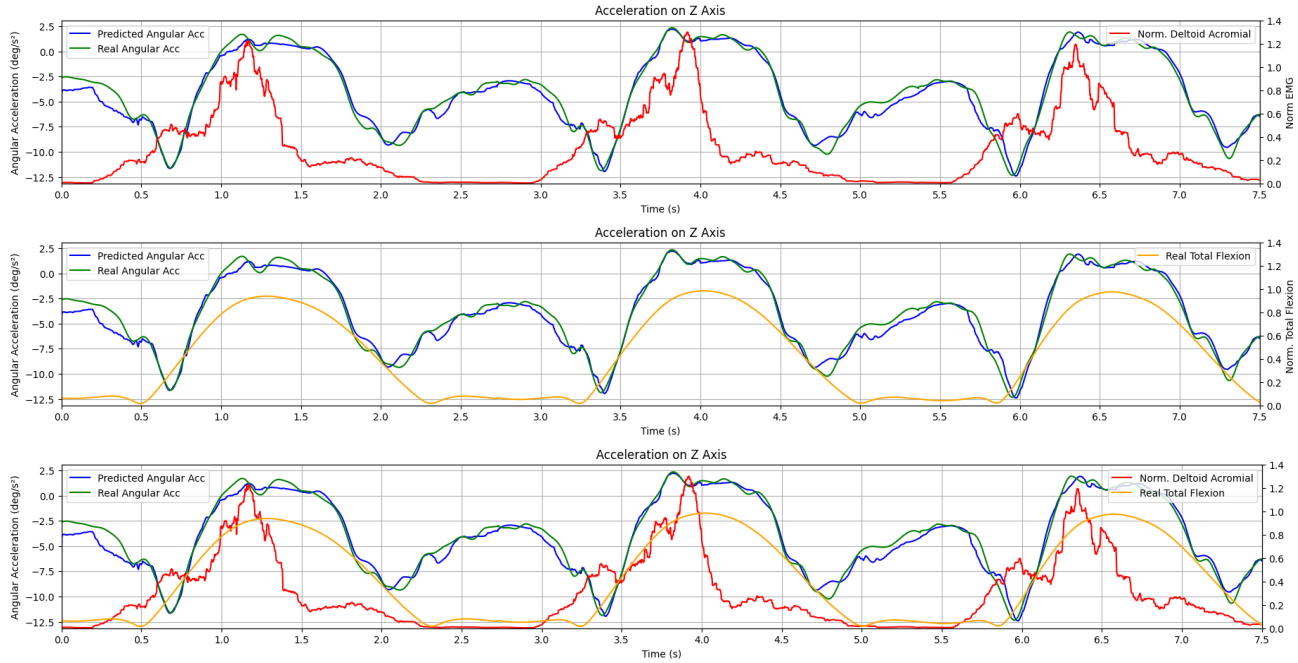

Fig.5. Motion Intention Prediction with Measured Humeral Acceleration on Z axis.

TABLE III. METHOD'S ACCURACY

Axis	*Average*	*Standard Deviation*	*Dimensional*
Unfiltered Shoulder Angle Performance			
X	0.604	0.600	deg/s^2
Y	0.655	0.655	deg/s^2
Z	0.607	0.598	deg/s^2
Filtered Shoulder Angle Performance			
X	0.572	0.571	deg/s^2
Y	0.588	0.585	deg/s^2
Z	0.573	0.571	deg/s^2

TABLE IV. METHOD'S COMPUTATIONAL TIME

Element	*Average*	*Standard Deviation*	*Dimensional*
MB	3.658	1.433	ms
MF	1.195	0.594	ms
TOTAL	4.889	1.722	ms
NOTE: The total rubric is not the addition but the measurement of the entire calculation time.			

The humeral acceleration was measured by the MyoMotion accelerometers and compared with the one calculated; the details of the results are in Table 3. These accuracy values indicate promising performance in evaluating various motions across a broad range of shoulder mobility. However, errors are observed predominantly at maximal and minimum total flexion angles. At minimum total flexion, this error occurs because the principal drivers for shoulder motion are the rotator cuff muscles. Since the method lacks information from these muscles, it is challenging for the method to estimate over this range. At maximal total flexion, the shoulder moment arm change and muscle conditions contraction capacity differ from shoulder level contraction capacity. Also, subjects' variations in effort to reach maximal total flexion generate an overestimation or underestimation of motion intention, as illustrated in Fig. 5. Future improvements may involve modifying the neural network architecture to better account for these variations. The proposed method can incorporate additional maximum voluntary contraction (MVC) exercises to normalize the sEMG signals relative to the shoulder position, which may help reduce the observed discrepancies.

Furthermore, the program demonstrated sufficient processing speed, averaging 4.899 milliseconds per sample, as detailed in Table 4. Considering that sEMG typically precedes movement by 50-100 milliseconds [40], the program operates effectively within the required time window.

VI. CONCLUSION

This work introduces a novel method for real-time estimation of shoulder motion intention. The proposed method integrates a neuromusculoskeletal model with a neural network, leveraging the strengths of both approaches. The neural network benefits from physiological insights from the neuromusculoskeletal model, while the method gets tailored to individual physiological characteristics. The method successfully operates within the necessary time window and achieves satisfactory accuracy. Further, the method estimates the shoulder intention of motion in its entire range of motion. These results suggest the potential for further development to encompass more complex physiological aspects and a broader range of upper-limb movements.

REFERENCES

[1] B. Sheng, J. Zhao, Y. Zhang, S. Xie, and J. Tao, "Commercial device-based hand rehabilitation systems for stroke patients: State of the art and future prospects," *Heliyon*, vol. 9, no. 3, p. e13588, Feb. 2023, doi: 10.1016/j.heliyon.2023.e13588.

[2] K. Kiguchi, T. Tanaka, and T. Fukuda, "Neuro-Fuzzy control of a robotic exoskeleton with EMG signals," *IEEE Transactions on Fuzzy Systems*, vol. 12, no. 4, pp. 481–490, Aug. 2004, doi: 10.1109/tfuzz.2004.832525.

[3] K. L. Narayanan *et al.*, "Robotic devices for upper limb rehabilitation: A review," *Elsevier eBooks*, pp. 123–156, Jan. 2023, doi: 10.1016/b978-0-443-18460-4.00005-6.

[4] Z. Wei, Z. Zhang, and S. Q. Xie, "Continuous Motion Intention Prediction Using SEMG for Upper-Limb Rehabilitation: A Systematic Review of Model-Based and Model-Free Approaches," *IEEE Transactions on Neural Systems and Rehabilitation Engineering*, vol. 32, pp. 1487–1504, Jan. 2024, doi: 10.1109/tnsre.2024.3383857.

[5] K. Shirota, A. Kashiwagi, K. Kiguchi, and S. Nishikawa, "Wearable device to inhibit wrist dorsiflexion for improving movement form in table tennis backhand," *2022 IEEE/SICE International Symposium on System Integration (SII)*, pp. 429–434, Jan. 2024, doi: 10.1109/sii58957.2024.10417593.

[6] S. P. Sitole and F. C. Sup, "Continuous Prediction of human joint mechanics using EMG Signals: A review of Model-Based and Model-Free approaches," *IEEE Transactions on Medical Robotics and Bionics*, vol. 5, no. 3, pp. 528–546, Jul. 2023, doi: 10.1109/tmrb.2023.3292451.

[7] J. V. D. Santos, M. V. M. Ramis, V. M. Oliveira, and R. Z. Azzolin, "A survey on Mathematical modeling of muscle using for rehabilitation systems," *IECON 2020 the 46th Annual Conference of the IEEE Industrial Electronics Society*, Oct. 2019, doi: 10.1109/iecon.2019.8927318.

[8] T. S. Buchanan, D. G. Lloyd, K. Manal, and T. F. Besier, "Neuromusculoskeletal Modeling: Estimation of Muscle Forces and Joint Moments and Movements from Measurements of Neural Command," *Journal of Applied Biomechanics*, vol. 20, no. 4, pp. 367–395, Nov. 2004, doi: 10.1123/jab.20.4.367.

[9] T. K. K. Koo, A. F. T. Mak, and L. K. Hung, "In vivo determination of subject-specific musculotendon parameters: applications to the prime elbow flexors in normal and hemiparetic subjects," *Clinical Biomechanics*, vol. 17, no. 5, pp. 390–399, Jun. 2002, doi: 10.1016/s0268-0033(02)00031-1.

[10] A. Yataganbaba, E. Ceyhan, and G. Huri, "Shoulder Kinematics and Biomechanics," in *Springer eBooks*, 2022, pp. 23–36. doi: 10.1007/978-3-030-94702-6_4.

[11] A. Seth, R. Matias, A. P. Veloso, and S. L. Delp, "A Biomechanical Model of the Scapulothoracic Joint to Accurately Capture Scapular Kinematics during Shoulder Movements," *PLoS ONE*, vol. 11, no. 1, p. e0141028, Jan. 2016, doi: 10.1371/journal.pone.0141028.

[12] J. Rosen, M. Brand, M. B. Fuchs, and M. Arcan, "A myosignal-based powered exoskeleton system," *IEEE Transactions on Systems Man and Cybernetics - Part a Systems and Humans*, vol. 31, no. 3, pp. 210–222, May 2001, doi: 10.1109/3468.925661.

[13] J. C. Perry, J. Rosen, and S. Burns, "Upper-Limb powered exoskeleton design," *IEEE/ASME Transactions on Mechatronics*, vol. 12, no. 4, pp. 408–417, Aug. 2007, doi: 10.1109/tmech.2007.901934.

[14] E. K. Chadwick, D. Blana, A. J. Van Den Bogert, and R. F. Kirsch, "A Real-Time, 3-D musculoskeletal model for dynamic simulation of arm movements," *IEEE Transactions on Biomedical Engineering*, vol. 56, no. 4, pp. 941–948, Sep. 2008, doi: 10.1109/tbme.2008.2005946.

[15] Y. M. Aung, K. Anam and A. Al-Jumaily, "Continuous prediction of shoulder joint angle in real-time," *2015 7th International IEEE/EMBS Conference on Neural Engineering (NER)*, Montpellier, France, 2015, pp. 755-758, doi: 10.1109/NER.2015.7146733.

[16] A. Ehrampoosh, A. Yousefi-koma, S. S. Mohtasebi and M. Ayati, "EMG-based estimation of shoulder kinematic using neural network and quadratic discriminant analysis," *2016 4th International Conference on Robotics and Mechatronics (ICROM)*, Tehran, Iran, 2016, pp. 471-476, doi: 10.1109/ICRoM.2016.7886786.

[17] S. L. Delp *et al*., "OpenSim: Open-Source Software to Create and Analyze Dynamic Simulations of Movement," in *IEEE Transactions on Biomedical Engineering*, vol. 54, no. 11, pp. 1940-1950, Nov. 2007, doi: 10.1109/TBME.2007.901024.

[18] E. K. Chadwick, D. Blana, R. F. Kirsch and A. J. van den Bogert, "Real-Time Simulation of Three-Dimensional Shoulder Girdle and Arm Dynamics," in *IEEE Transactions on Biomedical Engineering*, vol. 61, no. 7, pp. 1947-1956, July 2014, doi: 10.1109/TBME.2014.2309727.

[19] C. E. Boettcher, K. A. Ginn, and I. Cathers, "Standard maximum isometric voluntary contraction tests for normalizing shoulder muscle EMG," *Journal of Orthopaedic Research®*, vol. 26, no. 12, pp. 1591–1597, Jun. 2008, doi: 10.1002/jor.20675.

[20] B. T. Kelly, W. R. Kadrmas, D. T. Kirkendall, and K. P. Speer, "Optimal normalization tests for shoulder muscle activation: An electromyographic study," *Journal of Orthopaedic Research®*, vol. 14, no. 4, pp. 647–653, Jul. 1996, doi: 10.1002/jor.1100140421.

[21] B. . -C. Tsai, W. . -W. Wang, L. . -C. Hsu, L. . -C. Fu and J. . -S. Lai, "An articulated rehabilitation robot for upper limb physiotherapy and training," *2010 IEEE/RSJ International Conference on Intelligent Robots and Systems*, Taipei, Taiwan, 2010, pp. 1470-1475, doi: 10.1109/IROS.2010.5649567.

[22] S. Moubarak, M. T. Pham, T. Pajdla, and T. Redarce, "Design and modeling of an upper extremity exoskeleton," in *IFMBE proceedings*, 2009, pp. 476–479. doi: 10.1007/978-3-642-03889-1_127.

[23] B. Hudgins, P. Parker and R. N. Scott, "A new strategy for multifunction myoelectric control," in *IEEE Transactions on Biomedical Engineering*, vol. 40, no. 1, pp. 82-94, Jan. 1993, doi: 10.1109/10.204774.

[24] E. R. Avila, S. E. Williams, and C. Disselhorst-Klug, "Advances in EMG measurement techniques, analysis procedures, and the impact of muscle mechanics on future requirements for the methodology," *Journal of Biomechanics*, vol. 156, p. 111687, Jun. 2023, doi: 10.1016/j.jbiomech.2023.111687.

[25] R. R. Neptune and S. A. Kautz, "Muscle activation and deactivation dynamics: the governing properties in fast cyclical human movement performance?," *Exercise and Sport Sciences Reviews*, vol. 29, no. 2, pp. 76–81, Apr. 2001, doi: 10.1097/00003677-200104000-00007.

[26] F. E. Zajac, "Muscle and tendon: properties, models, scaling, and application to biomechanics and motor control," *Critical Reviews in Biomedical Engineering*, vol. 17, no. 4, pp. 359–411, 1989, Available: https://pubmed.ncbi.nlm.nih.gov/2676342/

[27] A. M. Gordon, A. F. Huxley, and F. J. Julian, "The variation in isometric tension with sarcomere length in vertebrate muscle fibres," *The Journal of Physiology*, vol. 184, no. 1, pp. 170–192, May 1966, doi: 10.1113/jphysiol.1966.sp007909.

[28] R. Rockenfeller, M. Günther, and S. L. Hooper, "Muscle active force-length curve explained by an electrophysical model of interfilament spacing," *Biophysical Journal*, vol. 121, no. 10, pp. 1823–1855, Apr. 2022, doi: 10.1016/j.bpj.2022.04.019.

[29] L. M. Schutte, "Using musculoskeletal models to explore strategies for improving performance in electrical stimulation-induced leg cycle ergometry," PhD Thesis, Standford University, 1992.

[30] A. V. Hill, "The heat of shortening and the dynamic constants of muscle," *Proceedings of the Royal Society of London. Series B, Biological Sciences*, vol. 126, no. 843, pp. 136–195, Oct. 1938, doi: 10.1098/rspb.1938.0050.

[31] The MathWorks, Inc. (2022). *MATLAB version: 9.13.0 (R2022b)*. Accessed: January 01, 2023. Available: https://www.mathworks.com

[32] E. Otten, "A myocybernetic model of the jaw system of the rat," *Journal of Neuroscience Methods*, vol. 21, no. 2–4, pp. 287–302, Oct. 1987, doi: 10.1016/0165-0270(87)90123-3.

[33] X. Aubert, *Le couplage énergétique de la contraction musculaire*, Thèse d'agégation, Brussels: Arscia, 1956.

[34] J. E. Wood, S. G. Meek, and S. C. Jacobsen, "Quantitation of human shoulder anatomy for prosthetic arm control—I. Surface modelling," *Journal of Biomechanics*, vol. 22, no. 3, pp. 273–292, Jan. 1989, doi: 10.1016/0021-9290(89)90094-8.

[35] J. E. Wood, S. G. Meek, and S. C. Jacobsen, "Quantitation of human shoulder anatomy for prosthetic arm control—II. Anatomy matrices," *Journal of Biomechanics*, vol. 22, no. 4, pp. 309–325, Jan. 1989, doi: 10.1016/0021-9290(89)90045-6.

[36] N. Matsumura *et al.*, "Three-dimensional alignment changes of the shoulder girdle between the supine and standing positions," *Journal of Orthopaedic Surgery and Research*, vol. 15, no. 1, Sep. 2020, doi: 10.1186/s13018-020-01934-w.

[37] A. D. Fontana *et al.*, "The variance of clavicular surface morphology is predictable: an analysis of dependent and independent metadata variables," *JSES International*, vol. 4, no. 3, pp. 413–421, Jun. 2020, doi: 10.1016/j.jseint.2020.05.004.

[38] W. M. Bass, *Human Osteology: A Laboratory and Field Manual of the Human Skeleton*, Columbia, MO: Missouri Archaeological Society, 1971.

[39] P. M. Ludewig, V. Phadke, J. P. Braman, D. R. Hassett, C. J. Cieminski, and R. F. LaPrade, "Motion of the shoulder complex during multiplanar humeral elevation," *Journal of Bone and Joint Surgery*, vol. 91, no. 2, pp. 378–389, Jan. 2009, doi: 10.2106/jbjs.g.01483.

[40] K. Li, J. Zhang, L. Wang, M. Zhang, J. Li, and S. Bao, "A review of the key technologies for sEMG-based human-robot interaction systems," *Biomedical Signal Processing and Control*, vol. 62, p. 102074, Jul. 2020, doi: 10.1016/j.bspc.2020.102074.